Conical-cavity fiber optic sensor for temperature measurement in a steel furnace

Cielo, Paolo G.; Krapez, Jean-Claude; Lamontagne, M.; Thomson, J. G.; Lamb, Michael G.

Publisher's version / Version de l'éditeur:
https://doi.org/10.1117/12.60857
Optical Engineering, 32, 3, pp. 486-494, 1993-03-01

Conical-cavity fiber optic sensor for temperature measurement in a steel furnace

Paolo Cielo
Jean-Claude Krapez
Mario Lamontagne
National Research Council Canada
Industrial Materials Institute
75, De Mortagne Boulevard
Boucherville, Québec J4B 6Y4 Canada

John G. Thomson
Michael G. Lamb
Stelco Inc.
Hilton Works
Hamilton, Ontario L8N 3T1 Canada

Abstract. An integrating-cavity sensor for temperature measurement of the steel sheet in a continuous annealing furnace is described. The sensor includes a fiber optic cable for transmission of the infrared radiation from the sensor head within the furnace to the double-wavelength detection unit located outside the furnace. The sensor head includes a reflecting conical cavity positioned above the steel sheet to increase, and thus stabilize, the effective infrared emissivity of the sheet surface as well as to reduce spurious reflections from other sources within the furnace. The fiber optic cable is both decentered and tilted with respect to the cavity axis to minimize straight-reflection losses through the fiber cable gate. Preliminary results after in-furnace installation are described.

Subject terms: temperature sensors; infrared pyrometry; fiber optic sensors; integrating cavities.

Optical Engineering 32(3), 486–493 (March 1993).

1 Introduction

On-line temperature sensing is a challenging field of industrial instrumentation (Ref. 1, Sect. 7-2). Because the product whose temperature is to be monitored is often continuously moving, noncontact temperature sensors are most convenient. One of the main problems faced by noncontact pyrometric temperature measurement of metal sheets is related to the low and variable surface emissivity of the metal sheet. This in turn intensifies the problem of spurious reflections from nearby heat sources.[2–4]

A reflecting cavity fiber optic sensor was recently developed at our institute for on-line aluminum temperature monitoring.[5,6] In this paper we describe a high-temperature version with decentered conical cavity and its application to on-line temperature monitoring in a steel continuous annealing furnace.

Paper 12052 received May 7, 1992; revised manuscript received June 26, 1992; accepted for publication June 27, 1992. This paper is a revision of a paper presented at the SPIE conference on Thermosense XIV: An International Conference on Thermal Sensing and Imaging Diagnostic Applications, April 22–24, 1992, Orlando, Florida. The paper presented there appears (unrefereed) in SPIE Proceedings Vol. 1682.

2 Overview of Low-Emissivity Pyrometric Techniques

A number of techniques have been investigated to improve the reliability of radiometric temperature measurements of low-emissivity materials such as metal sheets. A multiwavelength spectral analysis of the emitted infrared radiation may be performed by searching for a correlation with Planck's emission curve if information is available on the spectral distribution of the emissivity.[7–12] However, either double-wavelength or single low-wavelength pyrometers appear to provide comparable or better performances for the on-line inspection of metallic or composite surfaces.[13,14]

The introduction of an external light source for surface reflectivity evaluation has also been previously considered.[15–17] Such techniques, similar to polarization analysis methods,[18] are, however, difficult to apply to surfaces that are neither specular nor perfectly diffuse, while they still require shielding from ambient radiation. Alternatively, high-power lasers can be used to heat the inspected material in order to evaluate the absorptivity ratio,[19] or to get rid of the ambient reflection contribution.[20,21] However, the requirement for powerful lasers raises both costs and eye safety concerns in industrial applications.

Reflective shields can be introduced to improve the emissivity and remove stray radiation.[22] Either cooled or uncooled shields, as well as controlled radiators have been used in industrial thermometry.[23] Hemispherical reflectors in contact with the inspected surface have long been used to create near-blackbody conditions,[24] although the performance of such devices drops rapidly as the standoff distance (gap between the hemisphere and the inspected surface) increases.[25–27] Alternative reflector geometries, such as cylindrical cavities,[27] have been used to reduce standoff effects, while hemispherical reflectors with standoff control have recently been tested in industry.[28,29]

In this paper we present a conical-cavity sensor with a decentered and tilted fiber bundle. Applications to on-line steel temperature sensing are described.

3 Characterization of the Sensor

The temperature sensor was designed for operation in the continuous annealing furnace of a steel plant. One can assume, for this kind of application, that the steel sheet temperature is mainly between 500 and 800°C and that the vertical fluctuations of the horizontally moving sheet are of the order of ± 1 cm. A light reflectance analysis and radiometric emittance measurement with reference to a blackbody were performed on a number of steel sheets.[30] Typical near-IR emittance values were found to be of the order of 0.3 for clean steel sheets, corresponding to a normal reflectance of 0.7, with angular light scattering half-widths of the order of 0.5 deg in the machine direction and 2.5 deg in the cross-machine direction.

Figure 1 is a schematic diagram of the temperature sensor head. A fiber optic bundle assisted by a conical-shaped reflective cavity collects the infrared radiation from the steel sheet and transmits it to the detection unit (Fig. 2), which is located outside the furnace. As shown in Fig. 1, light beams exiting from the fiber bundle undergo multiple reflections and are mainly contained within the cavity. This results in a nearly 100% absorbance by the steel sheet if the top surface is highly reflecting, corresponding to nearly 100% effective emissivity of the steel sheet portion that is facing the cavity. A high effective emissivity leads to good signal repetitivity in spite of wide variations of the real sheet emissivity, which may change by a factor of more than two, depending on the steel surface chemistry and cleanness. Also shown in Fig. 1 are typical ray paths for light originating from outside spurious sources: It can be seen that spurious reflections tend to reach the fiber bundle at relatively wide angles with respect to the fiber axis. Most spurious light is thus not guided through the fibers whose numerical aperture was 0.2 in our case.

Figure 2 shows the double-wavelength detection module configuration. The infrared radiation transmitted through the fiber optic bundle is imaged onto two germanium detectors sensitive over the 1.2- and 1.6-μm (± 0.15 μm) spectral bands, respectively. This provides a good signal-to-noise ratio over the required temperature excursion range. The temperature is inferred from the detector output ratio through a calibration curve as discussed below.

The 10-m-long fiber bundle comprises nearly 40 QSF-AS silica fibers of 400 μm core and 480 μm cladding, which are held on a nearly 3.5-mm-diameter tip by high-temperature epoxy. This type of fiber has transmission losses smaller

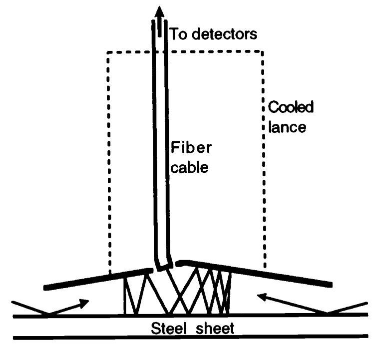

Fig. 1 Schematic diagram of the conical-cavity sensor head.

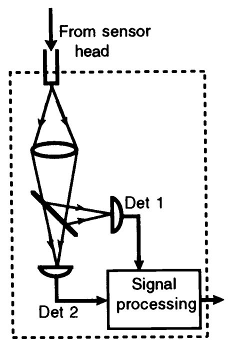

Fig. 2 Schematic diagram of the detection module of the temperature sensor.

than 1 dB/m in the 1- to 2-μm spectral range,[5] so that the attenuation due to the optical fibers is quite acceptable. Cooling of the fiber bundle tip is insured by thermal conduction to the cooled metal enclosure, whose temperature seldom exceeds 100°C during operation within the furnace. High operation temperatures may, however, affect the spectral transmittivity of the optical fibers, requiring in some cases an additional thermocouple within the fiber bundle to correct the sensor output.[31] Spectral FTIR scans were thus obtained through a 10-m-long fiber, an 8-m-portion of which was held in an oven at variable temperatures. Typical spectra are shown in Fig. 3.

The fiber transmittance is indeed affected by temperature, possibly due to the temperature dependence of dopants or to temperature variations of the core-cladding refractive index ratio in the 20-cm-diam fiber loop, but the spectral attenuation in the 1.2- and 1.6-μm regions appears to be uniform, so that the double-wavelength sensor output should not be affected by the fiber temperature variations. Although our FTIR spectrometer is limited to wavelengths higher than 1.3 μm, we do not expect substantial variations of the transmittance behavior below such a limit for short fiber lengths.

The reflective conical cavity has a diameter of 20 cm and a center vertex of 82.5 deg, or a 7.5-deg angle of the meridional profile with a flat sheet. A conical shape was preferred to a double wedge[5] partly because of its improved performance and partly because of cooling convenience with a single-block cylindrically symmetric cavity. The gold-plated copper reflector is normally standing over the steel sheet at a standoff distance (H in Fig. 4) of nearly 2.5 cm. At such a distance, the temperature perturbation introduced by the cooled sensor on the moving steel sheet (dwell time of the sheet underneath the sensor smaller than 0.1 s) is negligible. The performance of this cavity in terms of effective emissivity to spurious reflections will now be analyzed.

4 Theory

4.1 *Multiple Reflection Model*

A Monte-Carlo model was used to evaluate the performances of the conical-cavity sensor for different values of relevant parameters. The following properties were assumed for the steel sheet in all computations:

1. Emissivity $\varepsilon_M = 0.28$, independent of the observation angle (this approximation is acceptable in a first approximation since the experimental data show only a small increase of the sheet emissivity for observation angles up to 70 deg, a value that is seldom reached by the multiply reflected beam).
2. The reflectivity of the sheet takes into account its anisotropic topography due to directional rolling:
   a. A Gaussian-distributed light scattering pattern of half-width equal to 2.5 deg is assumed in the cross-machine direction.
   b. A similar distribution is assumed in the longitudinal direction, but with a half-width of only 0.5 deg.
   c. The light-scattering grooves on the sheet surface are themselves assumed to follow a direction that is itself defined by a normal distribution of 0.25 deg half-width.

The reflector was assumed to be perfectly specular with a reflectivity of 0.95. The acceptance angle of the optical fibers collecting the IR radiation corresponded to a 0.2 numerical aperture.

The radiative flux that is emitted by the different surfaces and finally collected by the fibers can be expressed by

$$\begin{aligned}\Phi_{\mathrm{em}} &= \int_{S_0}\int_{\Omega_0^F} \varepsilon_0^{(F)} L^0(T_0)\cos\theta_0^{(F)}\,d\Omega_0^{(F)}\,ds_0\\ &+\int_{\Omega_0^F}\int_{S_1}\int_{\Omega_1^0}[\varepsilon_1^{(0)}L^0(T_1)\cos\theta_1^{(0)}\,d\Omega_1^{(0)}\,ds_1]\rho_0^{1,F}\cos\theta_0^{(F)}\,d\Omega_0^{(F)}\\ &+\int_{\Omega_0^F}\int_{\Omega_1^0}\int_{S_2}\int_{\Omega_2^1}\{[\varepsilon_2^{(1)}L^0(T_2)\cos\theta_2^{(1)}\,d\Omega_2^{(1)}\,ds_2]\rho_1^{2,0}\\ &\times\cos\theta_1^{(0)}\,d\Omega_1^{(0)}\}\rho_0^{1,F}\cos\theta_0^{(F)}\,d\Omega_0^{(F)}+\cdots\ ,\end{aligned} \tag{1}$$

where

- the surface element ds_j is seen from ds_i at an angle of incidence $\theta_i^{(j)}$ and in a $d\Omega_i^{(j)}$ solid angle (F indicates the fiber bundle)
- $L^0(T_i)$ is the blackbody spectral radiance at the temperature T_i that prevails at the surface element ds_i
- $\varepsilon_i^{(j)}$ is the emissivity at ds_i in the direction of the surface element ds_j

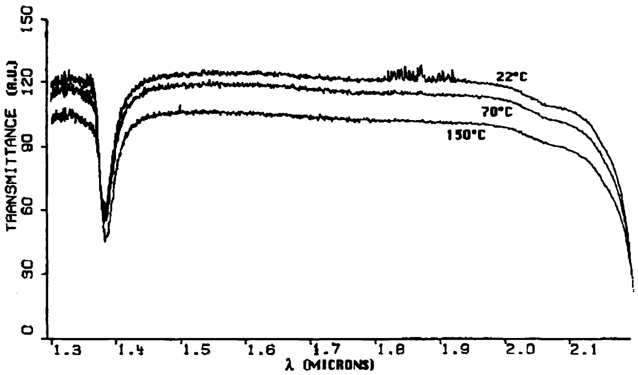

Fig. 3 Spectral transmittance of a QSF-AS optical fiber, with reference to a shorter fiber length, when the fiber temperature is raised to the indicated temperatures.

- $\rho_i^{j,k}$ is the reflectivity on ds_i per unit solid angle for a light bundle coming from ds_j and reflected toward ds_k
- Ω_i^j means that the integration is carried out with respect to $d\Omega_i^{(j)}$ over the hemisphere portion of the surface S_j, which is visible from ds_i.

By using Bouguer's identity; $\cos\theta_i^{(j)}\,d\Omega_i^{(j)}\,ds_i=\cos\theta_j^{(i)}\,d\Omega_j^{(i)}\,ds_j$, the previous expression becomes

$$\begin{aligned}\Phi_{\mathrm{em}} &= \int_{S_F}\int_{\Omega_F^0}\varepsilon_0^{(F)}L^0(T_0)\cos\theta_F^{(0)}\,d\Omega_F^{(0)}\,ds_F\\ &+\int_{S_F}\int_{\Omega_F^0}\int_{\Omega_0^1}[\varepsilon_1^{(0)}L^0(T_1)\cos\theta_0^{(1)}\,d\Omega_0^{(1)}]\rho_0^{1,F}\cos\theta_F^{(0)}\,d\Omega_F^{(0)}\,ds_F\\ &+\int_{S_F}\int_{\Omega_F^0}\int_{\Omega_0^1}\int_{\Omega_1^2}\{[\varepsilon_2^{(1)}L^0(T_2)\cos\theta_1^{(2)}\,d\Omega_1^{(2)}]\rho_1^{2,0}\\ &\times\cos\theta_0^{(1)}\,d\Omega_0^{(1)}\}\rho_0^{1,F}\cos\theta_F^{(0)}\,d\Omega_F^{(0)}\,ds_F+\cdots\ .\end{aligned} \tag{2}$$

By inverting the direction of the light rays, we can readily show that, for a radiance L_F emitted from the fibers within their angular aperture W_F, the absorption within the cavity is described by the expression

$$\begin{aligned}\Phi_{\mathrm{abs}} &= \int_{S_F}\int_{\Omega_F^0}L_F\alpha_0^{(F)}\cos\theta_F^{(0)}\,d\Omega_F^{(0)}\,ds_F\\ &+\int_{S_F}\int_{\Omega_F^0}\int_{\Omega_0^1}(L_F\alpha_1^{(0)}\cos\theta_0^{(1)}\,d\Omega_0^{(1)})\rho_0^{1,F}\cos\theta_F^{(0)}\,d\Omega_F^{(0)}\,ds_F\\ &+\int_{S_F}\int_{\Omega_F^0}\int_{\Omega_0^1}\int_{\Omega_1^2}[(L_F\alpha_2^{(1)}\cos\theta_1^{(2)}\,d\Omega_1^{(2)})\rho_1^{2,0}\\ &\times\cos\theta_0^{(1)}\,d\Omega_0^{(1)}]\rho_0^{1,F}\cos\theta_F^{(0)}\,d\Omega_F^{(0)}\,ds_F+\cdots\ ,\end{aligned} \tag{3}$$

where $\alpha_i^{(j)}$ is the absorptivity at ds_i for a radiation coming from the direction of the surface element ds_j, and where, again, Bouguer's identity was applied, as well as the Helmoltz principle of reciprocity, $\rho_i^{j,k}=\rho_i^{k,j}$.

A comparison of Eqs. (2) and (3) shows that, in the general nonisothermal case, the calculation of the absorbed flux F_{abs} may be used to evaluate the emitted flux F_{em}

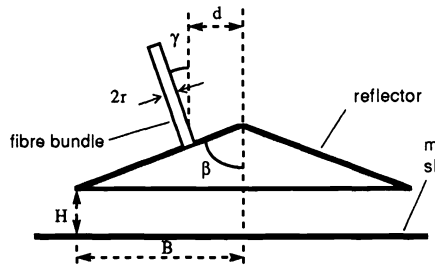

Fig. 4 Schematic cross-sectional diagram of the conical reflector.

provided L_F is chosen uniform and isotropic and that the values of the absorptivities $\alpha_i^{(j)}$ of each surface i are changed to $\alpha_i^{(j)}L^0(T_i)/L_F$ (if the surface directly seen by the fibers is isothermal at T_0, then L_F can be chosen as $L^0(T_0)$ so that $\alpha_i^{(j)}$ is changed to $\alpha_i^{(j)}L^0(T_i)/L^0(T_0)$, which now depends on the temperature of the first surface reached by the ray that, only after some reflections, reaches the surface i).

When each of the four main contributing surfaces or media is isothermal, the expression for the radiative flux transmitted by the fibers and collected by the detecting system can be simplified as follows:

$$\Phi_{\mathrm{em}} = \{\tilde{\varepsilon}_M L^0(T_M) + \tilde{\varepsilon}_R L^0(T_R) + \tilde{\varepsilon}_E L^0(T_E) + \tilde{\varepsilon}_F L^0(T_F)\}\Omega_F\left(1-\frac{\Omega_F}{4\pi}\right)s_F \ , \tag{4}$$

where the subscripts M, R, E, and F refer, respectively, to the metal sheet, the reflector, the environment, and the fiber bundle, whereas we define the weighing coefficients $\tilde{\varepsilon}\ldots$ as the corresponding apparent emissivities.

Comparisons between the reflector geometries were established by assuming the following as standard parameter values for all of them:

$H/B = 0.25$

$r/B = 0.03$

where (see Fig. 4)

- H is the gap between the reflector bottom and the metal sheet
- B is the radius of the reflector projection
- r is the radius of the fiber bundle section.

4.2 *Results of the Computations*

In a first series of computations, the fiber bundle was assumed to be in the center of the cavity ($d=0$ in Fig. 4).

The cone half-angle β was made to vary between 90 and 50 deg (90 deg corresponding to a perfectly flat reflector), while the fiber bundle angle γ could be varied between 0 and 40 deg. The steel sheet is first assumed to be normal to the axis of symmetry of the reflector; the effect of sheet tilting is analyzed later.

The effect of each of the parameters (β, γ, H/B, etc.) was analyzed by assuming a set of "standard" values for these parameters and by varying the value of each parameter individually while the others were kept constant at their standard value. For example, the standard value for the

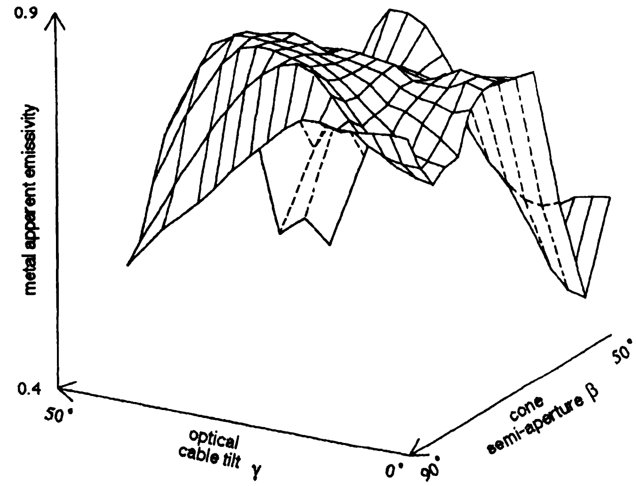

Fig. 5 Dependence of the effective emissivity on the values of the fiber cable tilting angle and on the half-aperture of the conical reflector, for a fiber pointing parallel to rolling.

fluttering parameter H/B is assumed to be equal to 0.25, while its value will in reality change between $\sim$0.1 and $\sim$0.4 because of actual sheet fluttering.

A first 3-D graph showing the effect on the reflector-assisted apparent sheet emissivity of the parameters γ (cable tilt angle) and β (half-aperture of the cone) is represented in Fig. 5, for standard values of the other parameters. The highest emissivity value is in this case

$$\tilde{\varepsilon}_M = 0.881 \qquad \text{for } \beta = 85 \text{ deg and } \gamma = 25 \text{ deg}$$

(the confidence interval half-width at 95% is of the order of 10^{-3}).

This graph corresponds to a cable orientation such that the rolling groove direction on the steel sheets is in the plane of Fig. 4 (fiber pointing parallel to rolling). When the grooves are perpendicular to the plane of Fig. 4 (fiber pointing normal to rolling) the apparent emissivity is slightly reduced with a maximum of $\tilde{\varepsilon}_M = 0.868 \pm 2\times10^{-3}$ for the same parameter combination as above.

In general, the efficiency of the reflector is slightly better when the fiber cable is tilted ($\gamma>0$): This decreases the exchange factor of the cable with itself. Tilting the cable, however, leads to a lower efficiency of the cone section opposed to the bundle (high stray-reflection losses through the reflector-sheet gap toward the right side on Fig. 4 for large values of γ and H/B). A possible solution would be an asymmetrical conical reflector, but its production would be problematic. The alternative approach consists of positioning the cable out of center by a distance d in the direction of the fiber tilt, as shown in Fig. 4.

Figure 6 shows a graph similar to that in Fig. 5, but with a fiber displacement $d=0.25$ B in the plane parallel to the rolling direction (the results are slightly inferior, but by only 1%, when the displacement is performed in a plane perpendicular to the rolling direction). By comparing the data of Figs. 5 and 6 one can see that the peak emissivity is almost identical (0.885 ± 10^{-3} compared to 0.881 ± 10^{-3}) but the real advantage of a fiber displacement is the substantial uniformity obtained in this case for the emissivity over a relatively wide range of the β and γ parameter var-

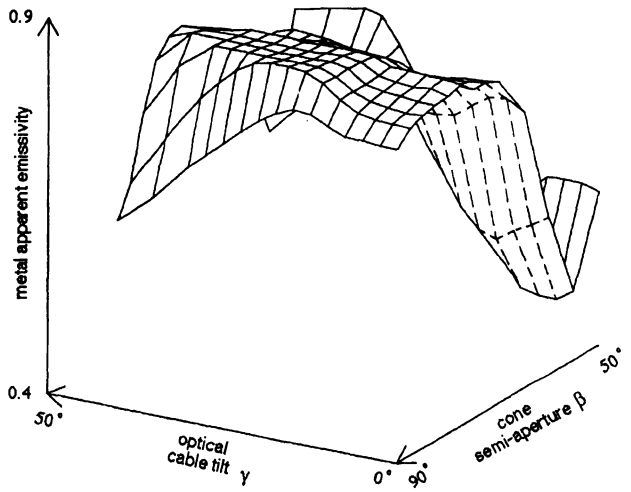

Fig. 6 Same as Fig. 5, but with the fiber bundle displaced out of center by 25% ($d/B = 0.25$ in Fig. 4).

iations. Such a uniformity relaxes the geometrical accuracy required in the reflector manufacturing and alignment, while making the performance less sensitive to the sheet fluctuations.

In view of these results, and due in part to space limitations in the cooled lance, we chose a fiber displacement $d = 0.15$ B and a $\beta = 82.5$ deg, $\gamma = 17.5$ deg couple such that the resultant emissivity is close to the peak value. Such parameters gave best results when taking into account the following range of in-furnace sheet geometry:

- the variations of the sheet fluttering parameter H/B between 0.05 and 0.6
- a tilting of the steel sheet with respect to the reflector axis by -2, 0, and $+2$ deg.

Figure 7 shows the sensitivity to sheet fluttering of the cavity with the (β, γ) couple of values mentioned above. In this figure, the effective emissivity and the contribution due to the environment (i.e., the stray reflectance losses through the reflector-to-sheet gap, or equivalently the relative amount of spurious radiation due to external infrared sources; the environment contribution should obviously be minimized as the amount of radiation from outside infrared sources is hardly predictable) are plotted vs. the sheet fluttering parameter H/B for three different angles of steel sheet tilt. It should be recalled that in the absence of the reflector, the steel emissivity would be 0.28 and the environment apparent emissivity 0.72 (blackbody reflecting once on the metal).

It can be concluded that for a $\beta = 82.5$ deg, $\gamma = 17.5$ deg couple the apparent emissivity of the steel sheet is more than tripled, while the outside contribution is smaller than 3.5×10^{-3} for a sheet fluttering parameter H/B in the range [0.1, 0.4] of normal operation.

We finally calculated the apparent emissivity for different values of the nominal sheet emissivity, keeping, however, the same Gaussian distribution for the radiation scattering pattern. The results are reported on Fig. 8. As an example, if the nominal steel sheet emissivity changes from 0.25 to

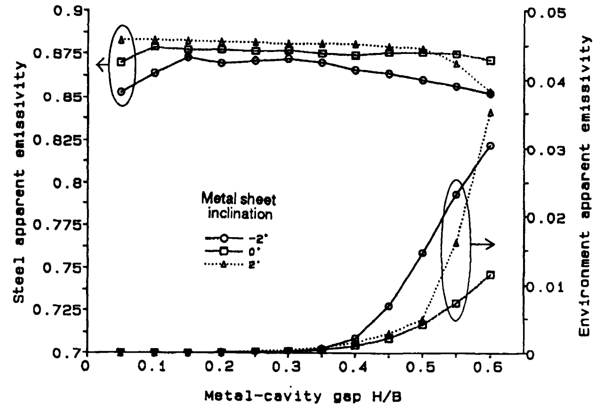

Fig. 7 Plot of the steel sheet apparent emissivity and of the external environment perturbation vs. the sheet fluttering parameter H/B for different values of the sheet tilt and for $\beta = 82.5$ deg and $\gamma = 17.5$ deg.

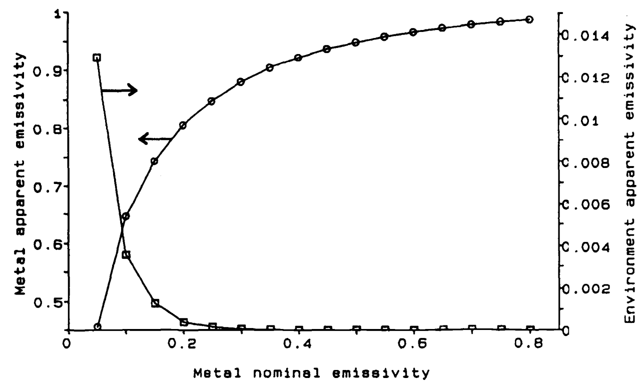

Fig. 8 Metal and environment apparent emissivities versus metal nominal emissivity with $\beta = 82.5$ deg, $\gamma = 17.5$ deg, and $d/B = 0.15$.

0.5, the apparent emissivity would increase by only 11% from 0.85 to 0.95. This would result in only a $\sim 1\%$ temperature error if the metal is at 1000 K and if a single-wavelength pyrometer at 1.5 μm is used.

5 Experimental Results

5.1 *Comparison of Blackbody and Steel Sheet Tests*

The temperature sensor was calibrated using a blackbody source. The ratio of detector 1 (1.2 μm) and detector 2 (1.6 μm) was recorded over a temperature range of 500 to more than 800°C, and a polynomial fit of the data points was obtained, providing the calibration curve to transform the sensor output into a temperature reading. Such an approach is both powerful (taking into account fiber transmission losses, detector spectral response, etc.) and flexible because the calibration curve can be readily updated by modifying the calibration constants. Needs for calibration update might arise because, e.g., of detector aging or sensor degradation with time. However, moderate accumulation of spectrally neutral specks on the optical surfaces (e.g., the fiber bundle tip or the reflector surfaces) should not affect the calibration curve because a similar attenuation of the two detector signals does not affect their ratio.

Table 1 Ratio signals obtained for different temperatures of the blackbody source.

Temperature (°C)	D_1 / D_2 with blackbody
550	0.254
600	0.316
650	0.385
700	0.453
750	0.540

A few data points recorded within the blackbody source are shown in Table 1 (the fiber optic tip was in this case positioned directly in front of the blackbody). Also, shown in Fig. 9, is a comparison between the pyrometer reading of the temperature of steel sheets and the output from thermocouples attached to the sheets. In this case the readings were made using the reflecting cavity at $H/B = 0.188$ with the voltage ratio D_1/D_2 converted to temperature by the blackbody calibration. Tests were made on both oxidized and bright surfaces to assess the emissivity independence of the measurements. The agreement between the pyrometer and the thermocouples is very good over the range 520 to 800°C, in most cases within the thermocouple error. In the case of the oxidized surface, the slight difference, or shift upward of 3 to 10°C, in the pyrometer output can be attributed to location of the thermocouples on the opposite surface of the 3.2-mm-thick sheet during the test in free cooling. The temperature differences noted between thermocouples positioned along a radius of the test sheet indicated that the pyrometer measured temperature in the region immediately below the fiber optic tip. The pyrometer does not average the temperature covered by the cavity.

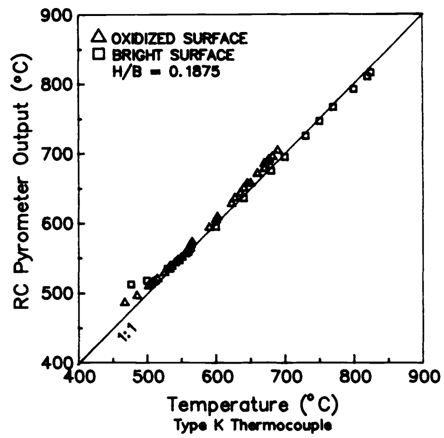

Fig. 9 Plot of the reflecting cavity pyrometer output versus temperature of oxidized and bright steel surfaces.

5.2 *In-Furnace Results*

The reflecting cavity (RC) pyrometer was installed to measure strip temperature at the soaking zone exit in the furnace of Stelco Steel's No. 2 continuous annealing line. This facility recrystallization anneals a light-gauge, cold-rolled sheet, primarily for tinplate applications, at speeds up to 335 m/min. The strip is at the hottest point in the annealing cycle exiting the soaking zone, and accurate measurement and regulation of this temperature is critical to grain size and hardness control. The strip temperature at this location is conventionally measured by a commercially available pyrometer based on a PbS detector and operating at 2.0 to 2.6 μm. The emissivity setting on this pyrometer is maintained at 0.4.

A comparison of the output from the reflecting cavity pyrometer and the conventional pyrometer is shown in Fig. 10 for approximately 2 h around a line stop. Preceding the line stop, the RC pyrometer follows the output of the conventional instrument with a constant offset of approximately 40°C. The RC pyrometer typically reads lower temperatures than the conventional pyrometer, due to the influence of reflected ambient heat on the latter. Immediately following the line stop, the temperature reading from the conventional pyrometer undergoes some instability not experienced by the RC pyrometer. This is understandable in terms of fluctuating strip emissivity on the material stalled upstream in the process, to which surface cleaning and annealing operations are applied nonuniformly.

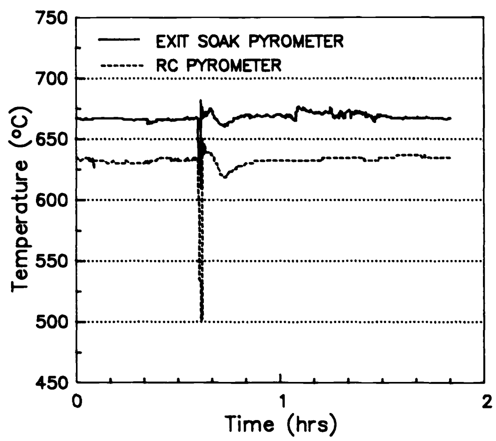

Fig. 10 On-line comparison of reflecting cavity and conventional pyrometer outputs showing emissivity instability effects.

The reflecting cavity pyrometer output is sensitive to standoff distance, as predicted in Fig. 7 and shown in Fig. 11. The temperature reading is stable up to $H/B \approx 0.6$, above which a positive deviation peaks around $H/B = 1.5$ before decreasing continuously. This behavior results from the combined effect of increasing ambient reflections and loss of cavity efficiency with increasing distance from the steel.

A check of the directional sensitivity of the RC pyrometer relative to the strip rolling direction was made to assess the effect of anisotropic reflectivity. Rotating the pyrometer ± 90 deg from the usual cable orientation recommended in Sec. 4.1 produced no change in measured temperature.

6 Conclusion

A conical-cavity, decentered fiber optic sensor has been developed for temperature measurement of steel sheets in a continuous annealing furnace. Geometrical parameters were optimized and the sensor performance was evaluated in terms of effective emissivity and background protection through a Monte Carlo simulation. The sensor was installed in a steel furnace and the preliminary results were satisfactory.

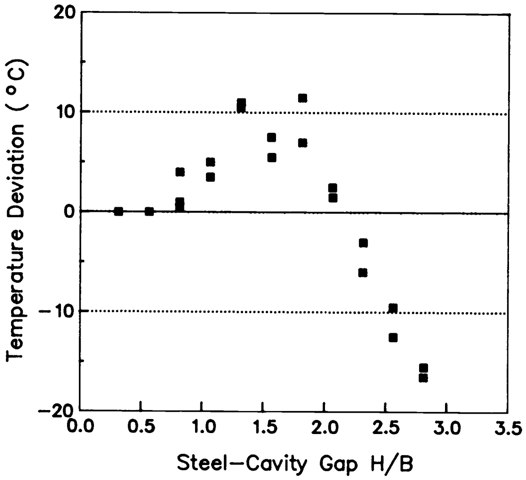

Fig. 11 Effect of standoff distance on the reflecting cavity temperature reading as observed on-line.

Acknowledgment

The authors gratefully acknowledge B. Gauthier of NRC-IMI for useful discussions during the development of the sensor electronics.

References

1. P. Cielo, *Optical Techniques for Industrial Inspection,* Academic, Boston (1988).
2. J. E. Roney, "Steel surface temperature measurement in industrial furnaces by compensation for reflected radiation errors," in *Temperature, its Measurement and Control in Science and Industry,* J. F. Schooley, Ed., Vol. 5, pp. 485–489, Am. Inst. Phys., New York (1982).
3. D. P. DeWitt, "Inferring temperature from optical radiation measurement," *Op.* Eng. **25,** 586–601 (1986).
4. F. A. Mihalow, "Radiation thermometry in the steel industry," in *Theory and Practice of Radiation Thermometry,* D. P. DeWitt and G. D. Nutter, Eds., pp. 861–904, Wiley-Interscience, New York (1988).
5. J.-C. Krapez, C. Bélanger, and P. Cielo, "A double-wedge reflector for emissivity enhanced pyrometry," *Meas. Sci. Technol.* **1,** 857–864 (1990).
6. J.-C. Krapez, P. Cielo, and M. Lamontagne, "Reflecting-cavity IR Temperature sensors: an analysis of spherical conical and double-wedge geometries," *Proc. SPIE* **1320,** 186–201 (1990).
7. J. L. Gardner, T. P. Jones, and M. R. Davies, "A six-wavelength radiation pyrometer," *High Temp.–High Press.* **13,** 459–466 (1981).
8. G. B. Hunter, C. D. Allemand, and T. W. Eagar, "Multiwavelength pyrometry: an improved method," *Opt. Eng.* **24,** 1081–1085 (1985).
9. J.-P. Hiernaut, F. Sakuma, and C. Ronchi, "Determination of the melting point and the emissivity of refractory metals with a six-wavelength pyrometer," *High Temp.–High Press.* **21,** 139–148 (1989).
10. M. A. Khan, C. Allemand, and T. W. Eagar, "Noncontact temperature measurement, I: interpolation based techniques," *Rev. Sci. Instrum.* **62,** 392–402 (1991).
11. M. A. Khan, C. Allemand, and T. W. Eagar, "Noncontact temperature measurement, II: least squares based techniques," *Rev. Sci. Instrum.* **62,** 403–411 (1991).
12. V. N. Snopko, "Methods of optimal polychromatic pyrometry," *High Temp.* **25,** 724–729 (1988).
13. T. P. Jones, J. L. Gardner, and A. J. Richards, "Radiation pyrometers for temperature measurement during aluminum processing," *J. Phys. E: Sci. Instrum.* **20,** 615–621 (1987).
14. D. P. DeWitt and R. E. Rondeau, "Measurement of surface temperatures and spectral emissivities during laser irradiation," *J. Thermophys.* **3,** 153–159 (1989).
15. A. Stein, "Laser pyrometry," in *Proc. 6th ICALEO Conf.,* G. Kychakoff, Ed., pp. 29–35, Springer, Berlin (1987).
16. H. G. Kraus, "Optical spectral radiometric/laser reflectance method for noninvasive measurement of weld pool surface temperature," *Opt. Eng.* **26,** 1183–1190 (1987).
17. E. S. Cameron, "Laser assisted remote temperature measurement," *Proc. SPIE* **1044,** 155–162 (1989).
18. R. G. Rudolph, "Polaradiometer: a polarization technique for temperature measurement," in *Theory and Practice of Radiation Thermometry,* D. P. DeWitt and G. D. Nutter, Eds., pp. 553–564, Wiley-Interscience, New York (1988).
19. D. P. DeWitt and H. Kunz, "Theory and technique for surface temperature determinations by measuring the radiance temperatures and the absorptance ratio for two wavelengths," in *Temperature: Its Measurements and Control in Science and Industry,* H. H. Plumb, Ed., Vol. 4, pp. 599–610, ISA, Pittsburgh (1972).
20. T. Loarer, J.-J. Greffet, and M. Huetz-Aubert, "Non contact surface temperature measurement by means of a modulated photothermal effect," *Appl. Opt.* **29,** 979–987 (1990).
21. A. Lothon, Y. Denayrolles, and A. Kleitz, "A novel pyrometer using photothermal effect and fiber optics," *Proc. SPIE* **1313,** 238–243 (1990).
22. A. Ono, "Methods for reducing emissivity effects," in *Theory and Practice of Radiation Thermometry,* D. P. DeWitt and G. D. Nutter, Eds., pp. 565–624, Wiley-Interscience, New York (1988).
23. T. Iuchi, "Recent advances and research activities in Japan," in *Applications of Radiation Thermometry,* J. C. Richmond and D. P. DeWitt, Eds., STP 895, pp. 121–150, ASTM, Philadelphia (1985).
24. M. D. Drury, K. P. Perry, and T. Land, "Pyrometers for surface-temperature measurement," *J. Iron Steel Inst. London* **169,** 245–255 (1951).
25. R. E. Bedford, C. K. Ma, Z. Chu, and Y. Sun, "Calculation of the radiant characteristics of a plane diffuse surface covered by a specular hemisphere," *J. Phys. E: Sci. Instrum.* **21,** 785–791 (1988).
26. R. E. Bedford, C. K. Ma, Z. Chu, and Y. Sun, "Calculation of the effective emissivity of a diffuse plane surface below a specular hemisphere," *High Temp.–High Press.* **21,** 211–218 (1989).
27. T. Iuchi and R. Kusaka, "Two methods for simultaneous measurement of temperature and emittance using multiple reflection and specular reflection, and their applications to industrial processes," in *Temperature: Its Measurement and Control in Science and Industry,* J. F. Schooley, Ed., Vol. 5, pp. 491–503, Am. Inst. Phys., New York (1982).
28. D. Ramelot, J. M. Ludovicy, C. Stolz, and J. P. Fischbach, "Capteurs industriels pour applications basses temperatures," *Rev. Gen. Therm. Fr.* **322,** 517–524 (1988).
29. G. Heitz, "Tôle-voûte deux miroirs: mesure de temperature dans les fours de recuit continu," *Rev. Gen. Therm. Fr.* **322,** 511–515 (1988).
30. J.-C. Krapez, M. Lamontagne, and P. Cielo, "Interim report on the development of a reflective-cavity fiber optic temperature sensor," Report RT89-404-08C, NRC-IMI, Boucherville, Québec (1989).
31. M. Lucas, "A fiber-optic pyrometer for tuyère temperature measurement," *ISA Trans.* **27**(1), 1–8 (1988).

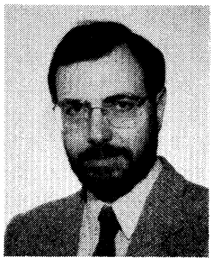

Paolo Cielo received his PhD degree in physics from Laval University, Québec, in 1977. Prior to joining the National Research Council of Canada, Industrial Materials Institute, in 1980, he was affiliated with Bell-Northern Research, Ottawa, and with the Defence Research Establishment Atlantic in Dartmouth, Nova Scotia. Dr. Cielo has authored more than 100 papers, 15 industrial patents, and a book on optical inspection. He is a fellow of the Optical Society of America.

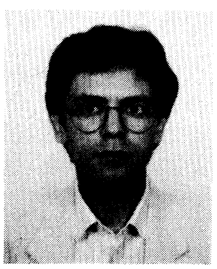

Jean-Claude Krapez received his Doctoral degree in thermal sciences from the Ecole Centrale de Paris in 1991. From 1986 to 1992 he was a research associate at the Industrial Materials Institute in Boucherville, Canada, where his research activities were in the field of pyrometry and thermal characterization. In 1992 he joined the Office National d'Etudes et de Recherches Aérospatiales in Châtillon, France, where he is pursuing research on thermal nondestructive evaluation.

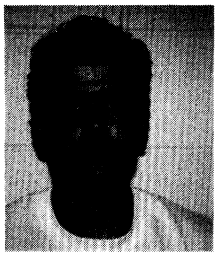

Mario Lamontagne received his diploma in physical technology from La Pocatière College, Québec, in 1979. After one year with the spectrometer manufacturer Bomem, Québec, he joined the National Research Council, Industrial Materials Institute, where he has since been active in the development of optical sensors for industrial control.

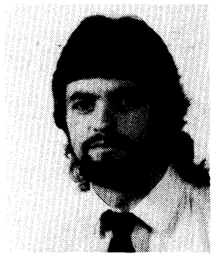

Michael G. Lamb obtained his diploma in mechanical engineering technology in 1986 from Mohawk College of Applied Arts and Technology, Hamilton, Ontario. As a research analyst in Stelco Steel's Research and Development Department since graduation, he has been involved in a wide range of process development and improvement projects in Stelco's Cold Mill.

John G. Thomson joined the Research and Development Department of Stelco in 1981 after graduating from McGill University with degrees in commerce and engineering metallurgy. His current technical interests are centered on the production of specific mechanical properties in steel strip for packaging, construction, electrical, and automotive applications.